Am J Transl Res 2022;14(1):534-553
www.ajtr.org /ISSN:1943-8141/AJTR0135798

Original Article

Adiponectin improves the therapeutic efficacy of mesenchymal stem cells by enhancing their engraftment and survival in the peri-infarct myocardium through the AMPK pathway

Xia-Qiu Tian[1], Xiao-Song Qian[2], Hong Wang[1], Yue-Jin Yang[3]

[1]Center for Cardiac Intensive Care, Beijing Institute of Heart, Lung and Blood Vessel Diseases, Beijing Anzhen Hospital, Capital Medical University, Beijing 100029, China; [2]Institute of Uro-Nephrology, Beijing Chaoyang Hospital, Capital Medical University, Beijing 100020, China; [3]State Key Laboratory of Cardiovascular Disease, Fuwai Hospital, National Center for Cardiovascular Diseases, Chinese Academy of Medical Sciences and Peking Union Medical College, Beijing 100037, China

Received May 29, 2021; Accepted December 8, 2021; Epub January 15, 2022; Published January 30, 2022

Abstract: Poor viability of transplanted mesenchymal stem cells (MSCs) within the ischemic heart has limited their therapeutic potential for cardiac repair. We have previously shown that adiponectin (APN) treatment inhibits MSCs apoptosis under ischemic conditions *in vitro*. In this study, we investigated whether APN promoted the survival of MSCs *in vivo* and further contributed to cardiac repair in a rat model of acute myocardial infarction (AMI) by activating the adenosine monophosphate-activated protein kinase (AMPK) signaling pathway. Rats were randomized into six groups: the sham, AMI control, and four other groups that were subjected to AMI followed by treatment with MSCs, APN, APN + MSCs, and APN + MSCs + AMPK inhibitor, respectively. The engraftment and survival of MSCs were detected using both immunofluorescence staining and qPCR. Cardiac function was assessed using echocardiography and left heart catheterization. H&E staining and immunohistochemical staining for MHC-II and CD206 were performed to assess the infiltration of inflammatory cells. Immunostaining for the smooth muscle cell marker α-smooth-muscle actin (α-SMA) and endothelial cell marker CD31 was performed to assess arteriogenesis and angiogenesis. APN treatment significantly enhanced the engraftment and survival rate of transplanted MSCs and further improved cardiac function and led to reduced infarct size compared with MSCs treatment alone at 4 weeks after AMI. Combined administration of APN and MSCs noticeably suppressed the inflammatory response by specifically promoting the shift of infiltrated macrophages to an less-inflammatory phenotype. Combined administration of APN and MSCs also significantly inhibited cardiomyocyte apoptosis and increased arteriogenesis and angiogenesis in the peri-infarct myocardium compared with MSCs transplantation alone. These protective effects of APN were associated with AMPK phosphorylation and were partially reversed by AMPK pathway inhibitors. Our results are the first to show that APN is able to effectively improve the survival and therapeutic efficacy of transplanted MSCs after AMI through AMPK activation. APN has the potential to be utilized for stem cell-based heart repair after AMI.

Keywords: Mesenchymal stem cell, adiponectin, acute myocardial infarction, AMPK

Introduction

Stem cell therapy has been recognized as an attractive therapeutic option to treat cardiovascular diseases in recent decades [1-3], and mesenchymal stem cells (MSCs) are the most promising stem cell types due to their ability to help repair the injured heart through multiple mechanisms [4, 5]. However, limited improvement has been reported for the left ventricular ejection fraction (LVEF) after stem cell transplantation for acute myocardial infarction (AMI) [6, 7]. This slight improvement was probably attributed to the limited engraftment and retention of MSCs in the infarcted myocardium. Moreover, the low survival rate of transplanted MSCs after exposure to a hostile environment, including inflammation, various proapoptotic factors, and low vascularization, is still a main hurdle that limits the therapeutic potential of

MSCs [8]. Therefore, developing strategies to attenuate the hostile environment and promote MSCs engraftment and survival would be paramount to enhance the effectiveness of cell therapy for myocardial infarction [9].

Adiponectin (APN) is an adipokine with pleiotropic cardioprotective effects [10, 11] and has shown great potential in improving the myocardial environment after AMI. APN activates the adenosine monophosphate-activated protein kinase (AMPK)-dependent signaling pathway [12] to exert its cardioprotective effects [13], including the prevention of myocardial ischemic-reperfusion injury [14]. APN supplementation might protect the heart from the development of systolic dysfunction following ischemic myocardial infarction through its ability to suppress cardiac hypertrophy and interstitial fibrosis, increase capillary density and protect against cardiomyocyte apoptosis [15]. APN has also been proposed to participate in tissue regeneration and promote the survival of several stem cells [16-18], including the proliferation and migration of MSCs [19].

More importantly, our previous study verified that APN inhibits the apoptosis of MSCs induced by ischemic conditions and promotes the survival of MSCs *in vitro* via the AMPK pathway [20]. AMPK is involved in regulating the cellular energy status by modulating the phosphorylation state of its substrates [21]. Additionally, a recent study showed that APN stimulates exosome release to enhance the therapeutic effect of MSCs on pressure overload-induced heart failure [22]. However, it is not clear whether APN affects the microenvironment of the infarcted myocardium, and thus determine the fate of transplanted MSCs. The present study intended to further investigate the effect of APN on the survival and therapeutic efficacy of MSCs in a rat model of AMI *in vivo* and the involvement of the AMPK pathway in this process.

Materials and methods

Ethics statement

This study was performed in strict accordance with the Chinese guidelines for the care and use of laboratory animals. All animals received humane care, and the experimental protocol was approved by the Institutional Review Board of Beijing Anzhen Hospital (2021132X).

Animals and grouping

Eighty-five Sprague-Dawley rats (200-220 g, female) were randomized into six groups: sham operation group (sham, n=10), AMI control group (AMI, n=15), APN injection only group (APN, n=15), MSCs transplantation only group (MSCs, n=15), APN combined with MSCs group (APN + MSCs, n=15) and APN combined with MSCs and AMPK inhibitor Compound C group (APN + MSCs + AMPK inhibitor, n=15). 12 (16%) rats died during the AMI modeling procedure, and 7 (9.3%) died within the first week post-AMI. Another 6 rats were also excluded from the experiment because their baseline echocardiography data (1 week post-AMI) did not meet the prespecified criteria for successful induction of the AMI model (LVEF<60% and abnormal motion of the left ventricular wall). MSCs labeled with CM-DiI were injected through the tail vein at 24 hours post AMI. Globular APN (1 μg/g/d, Biovision, USA) was administered daily via intraperitoneal injection beginning at 20 minutes after AMI for 4 weeks as described previously [23]. Compound C (20 μg/g/d, Selleckchem, USA) was injected intraperitoneally once a day beginning 20 minutes after AMI until the end of the study.

MSCs isolation, culture, and delivery

Adult rat bone marrow MSCs were isolated and cultured as previously described [24]. Briefly, bone marrow was harvested from the tibia and femur of Sprague-Dawley rats (60-80 g, male) and plated into cell culture flasks with complete medium in an incubator set to 37°C and containing 5% CO_2 and 95% air. The complete medium consisted of Iscove's modified Dulbecco's medium (IMDM, Gibco, USA), 10% fetal bovine serum (Gibco, USA), and 1% penicillin-streptomycin (Gibco, USA). The D-glucose (dextrose) concentration in IMDM is 25 mM. All cells were used in the experiment at passage 3.

Before transplantation, MSCs were labeled with CellTracker CM-DiI (Molecular Probe, Invitrogen, USA) [25]. CM-DiI-labeled MSCs (2.0×10^6) in a total volume of 0.5 ml of phosphate-buffered saline (PBS) were injected through the tail vein at 24 hours post AMI, as

described previously [26]. The control group received the same volume of cell-free PBS.

Establishment of the acute myocardial infarction model

The AMI model was established in female SD rats as previously described [27]. Briefly, rats were anesthetized by administering an intraperitoneal injection of pentobarbital sodium (30 mg/kg) before the surgical procedure. Then, the chest was opened gently by performing a left thoracotomy, and the pericardium was removed to reach the left ventricular (LV) free wall. AMI was induced by permanent ligation of the proximal left anterior descending coronary artery (LAD) with a 6-0 polyester suture 1-2 mm from the tip of the left atrial appendage. The sham operation group underwent the same procedure without coronary ligation. Successful ligation of the LAD was confirmed by visual blanching of the distal site and by baseline echocardiography showing an LVEF<60% and abnormal motion of the left ventricular wall at 1 week post-AMI.

Detection of MSCs engraftment and survival with immunofluorescence staining

Hearts were harvested at 4 weeks after AMI to explore the role of APN in promoting MSCs survival following an intravenous infusion. Hearts were embedded in Tissue-Tek OCT compound (Sakura) and cut into 5 mm-thick serial sections, and nuclei were stained with DAPI. The sections were analyzed using a laser scanning confocal microscope (Leica, Germany). The excitation wavelengths were 561 nm and 405 nm for the detection of CM-DiI and DAPI, respectively. The numbers of labeled MSCs in 10 randomized high-power fields (×600) per animal were quantified by an independent researcher who was blinded to the groups.

Analysis of MSCs survival with quantitative real-time polymerase chain reaction (qPCR)

Quantitative real-time PCR (qPCR) was performed to identify the surviving transplanted MSCs based on the presence of a Y chromosome at 4 weeks post AMI. Briefly, DNA was extracted from heart tissues to obtain the qPCR template using the Genomic DNA Purification Kit (Promega) according to the manufacturer's instructions, and the concentration of the purified DNA was determined using spectrophotometry. Subsequently, qPCR was performed using specific primers for the sex-determining region of the Y chromosome (SRY) gene of the rat. β-Actin was used as a housekeeping gene for normalization. The sequences of the primers ultimately used were SRY-F, 5'-CATCGAAGGGTTAAAGTGCCA; SRY-R, 5'-ATAGTGTGTAGGTTGTTGTCC; β-actin-F, 5'-AGAAGCTGTGCTATGTTG; and β-actin-R, 5'-GTACTCCTGCTTGCTGATCC. The expression of the SRY gene was normalized using the standard comparative CT method with the formula $2^{-\Delta\Delta CT}$.

Assessment of cardiac function using echocardiography and catheterization

Transthoracic echocardiography was performed at 1 week (baseline) and 4 weeks (endpoint) after AMI with a 12-MHz phased-array transducer (Sonos 7500, Phillips). After two-dimensional images were obtained, the hearts were measured in M-mode from the parasternal long-axis view at the papillary muscle level. The left ventricular end-systolic diameter (LVESd) and end-diastolic diameter (LVEDd) were detected. The left ventricular ejection fraction (LVEF) and left ventricular fractional shortening (LVFS) were calculated using the following equations: LVEF (%) = $[(LVEDd)^3 - (LVESd)^3]/(LVEDd)^3 \times 100\%$, and LVFS (%) = (LVEDd - LVESd)/LVEDd ×100%. Variations in the LVEF and LVFS were calculated by subtracting the values at endpoints from baseline values.

Left heart catheterization was performed at 4 weeks after AMI to assess cardiac function. The left ventricular pressure curve was recorded, and the left ventricular end-diastolic pressure (LVEDP) and the left ventricular pressure maximal rate of rising and falling ($\pm dp/dt_{max}$) were recorded.

Histological assessment of the infarct size and inflammation

At 4 weeks post-AMI, the animals were sacrificed and heart tissues were collected. The hearts were fixed with 10% formalin for the preparation of paraffin sections. The paraffin sections were stained with Masson's trichrome and hematoxylin-eosin (H&E). The infarct sizes were calculated as infarct circumference divided by total left ventricular circumference.

H&E staining was performed to roughly observe inflammation in the peri-infarct region. Immunohistochemical staining for MHC-II (M1 marker) and CD206 (M2 marker) was performed to further evaluate the level and phenotype of infiltrating inflammatory cells, especially macrophages. The sections were processed as described above for the histological procedure and incubated overnight with primary rabbit anti-MHC-II (Abcam, 1:1,000 dilution) and CD206 (Abcam, 1:1,000 dilution) antibodies at 4°C followed by an incubation with a goat anti-rabbit IgG (Beyotime, China, 1:200 dilution) secondary antibody and color development with the DAB kit. Five randomly chosen fields in stained sections (×200) were examined under a microscope. The results of inflammatory cell infiltration were described as follows: the number of MHC-II$^+$ cells/total cells ×100% and CD206$^+$ cells/total cells ×100%.

Assessment of cardiomyocyte and MSCs apoptosis with the TUNEL assay

For the apoptosis analysis, TdT-mediated dUTP nick-end labeling (TUNEL) In Situ Cell Death Detection (Roche, Mannheim, Germany, 11772465001) was implemented according to the manufacturer's instructions. The samples were fixed with OCT medium. TUNEL-positive cells were examined under a fluorescence microscope at ×200 magnification in 5 randomly chosen fields. Nuclei were stained with DAPI and presented in blue, while apoptotic nuclei are presented green. The results are presented as the percentage of apoptotic cells to the total cells.

Determination of pro- and anti-inflammatory cytokine levels in heart tissues with ELISAs and qPCR

Quantitative immunoassays were performed to evaluate the expression of interleukin-6 (IL-6), tumor necrosis factor-α (TNF-α), and interleukin-10 (IL-10) in the peri-infarct area at the endpoint according to the manufacturer's protocol (R&D Systems, USA). Tissues from the peri-infarct regions of the myocardium were homogenized. IL-6, TNF-α, and IL-10 proteins supplied by the kit were used to plot the standard curves. The optical density of each sample was detected using an enzyme-labeling measuring instrument at a wavelength of 450 nm, and the concentration was determined from the standard curve. All measurements were repeated 3 times to obtain an arithmetic average.

Quantitative real-time PCR (qPCR) was performed to validate the expression of the IL-6, TNF-α, and IL-10 mRNAs. Total RNA was extracted from heart tissues using TRIzol reagent (Invitrogen, USA) according to the manufacturer's instructions. The cDNA templates were synthesized from total RNA using a TIANScript RT Kit (Qiagen, Germany). qPCR was performed with SYBR FAST qPCR Kit Master Mix (2×) Universal (KAPA, USA). β-Actin was used as a housekeeping gene for normalization. The reaction conditions were as follows: 95°C for 3 min, followed by 40 cycles of 95°C for 3 s and 63°C for 20 s. The primer sequences ultimately used in this study were IL-6-F, 5'-ACTTCCAGCCAGTTGCCTTCTTG; IL-6-R, 5'-TGGTCTGTTGTGGGTGGTATCCTC; TNF-α-F, 5'-ATGGGCTCCCTCTCATCAGTTCC; TNF-α-R, 5'-CCTCCGCTTGGTGGTTTGCTAC; IL-10-F, 5'-GGCAGTGGAGCAGGTGAAGAATG; IL-10-R, 5'-TGTCACGTAGGCTTCTATGCAGTTG; β-actin-F, 5'-GCTGTGCTATGTTGCCCTAGACTTC; and β-actin-R, 5'-GGAACCGCTCATTGCCGATAGTG. Data were normalized using the standard comparative CT method with the formula $2^{-\Delta\Delta CT}$.

Evaluation of arteriogenesis and angiogenesis using immunohistochemical and immunofluorescence staining

Vessel densities were evaluated in peri-infarct areas. Sections were fixed with 4% paraformaldehyde, rinsed with PBS, and blocked with 0.1% PBS-T containing 1% BSA. The sections were processed according to the aforementioned histological procedure and incubated overnight with primary rabbit anti-α-smooth muscle actin (α-SMA, Abcam, 1:1,000 dilution) antibodies at 4°C followed by an incubation with the goat anti-rabbit IgG (Beyotime, China, 1:200 dilution) secondary antibody and color development with the DAB kit. After an incubation with the rabbit anti-CD31 antibody (1:300, Abcam, Cambridge, MA) at 4°C overnight, sections were washed with PBS and incubated with an Alexa Fluor 488-conjugated goat (Cell Signaling Technology, Danvers, MA, #4412, 1:500) secondary antibody (R&D Systems, Minneapolis, MN, NL007, 1:100). After washing, the nuclei were counterstained with

DAPI (Invitrogen). The sections were analyzed under an FV1000 laser scanning confocal microscope (Olympus), and 5 random high-power fields were chosen per animal.

Detection of AMPK phosphorylation using immunohistochemistry

Immunohistochemical staining for phospho-AMPK (p-AMPK) was performed in the peri-infarct region of heart tissues. The sections were processed according to the aforementioned histological procedure and incubated overnight with a primary rabbit anti-p-AMPK antibody (Cell Signaling Technology, 1:1,000 dilution) at 4°C followed by an incubation with a goat anti-rabbit IgG (Beyotime, China, 1:200 dilution) secondary antibody and color reaction with the DAB kit. Five randomly chosen fields (×200) in the stained sections were examined under a microscope. The results of AMPK phosphorylation were reported as follows: the area of the positive signal for AMPK phosphorylation/total area ×100%.

Detection of AMPK phosphorylation using Western blot analysis

Heart tissues were extracted from peri-infarct regions of the myocardium for Western blot analysis at 4 weeks post-AMI. Protein concentrations were measured with a BCA assay. Fifty milligrams of protein lysate were resolved on SDS-PAGE gels, and transferred to nitrocellulose membranes (Life Technologies) that were subsequently blocked with 5% nonfat dry milk to detect AMPK and p-AMPK levels in the heart tissue. The following primary antibodies were used: β-actin (1:1000, Cell Signaling Technology, Danvers, MA), AMPK (1:1000, Cell Signaling Technology, Danvers, MA), and p-AMPK (1:1000, Cell Signaling Technology, Danvers, MA). Target protein signals were normalized to β-actin as a loading control (1:1000 dilution; Zhongshanjinqiao, China). After washing, the membranes were incubated for 1 h at room temperature with a blocking solution containing peroxidase-conjugated secondary antibodies. Next, the membranes were washed and processed for analysis using a Chemiluminescence Detection Kit (Pierce) according to the manufacturer's instructions. The densitometry analysis was completed using Quantity One software.

Statistics

All the data are described as the means±SD, and analyses were performed with GraphPad Prism software (Version 6.0c, GraphPad Software, La Jolla, CA). The statistical significance of differences among groups was evaluated with one-way ANOVA followed by a post hoc LSD test, and a value of $P<0.05$ was considered statistically significant.

Results

APN treatment facilitated the engraftment and survival of MSCs in the peri-infarct myocardium

Consistent with the protective effect of APN on MSCs observed *in vitro* in our previous study, APN treatment improved the engraftment and survival of transplanted MSCs *in vivo* at 4 weeks after infarction. As shown in **Figure 1A**, **1B**, few CM-DiI-positive cells were observed in the border zone of the ischemic myocardium in rats treated with MSCs alone. In comparison, the combined administration of APN and MSCs markedly increased the percentage of CM-DiI-positive cells in the peri-infarct myocardium (15.78±2.88% vs. 8.02±2.26%, $P<0.05$). In addition, as shown in **Figure 1C**, qPCR analysis verified that the expression of SRY-specific genes was significantly increased after the combined administration of APN and MSCs compared to MSCs treatment alone (2.74±0.43 vs. 1.00±0.21, $P<0.05$). These results suggested that APN treatment might increase the engraftment and survival of transplanted MSCs in postinfarct cardiac tissue.

Adjuvant APN treatment with MSCs transplantation improved cardiac function and attenuated adverse remodeling

According to the cardiac dimensions and functional results assessed with echocardiography, the AMI rats did not exhibit any differences at baseline between different groups, which validated the reliability and consistency of the established AMI models (Table S1). At 4 weeks after AMI, the rats treated with MSCs alone exhibited significantly increased changes in LVEF (ΔLVEF) and LVFS (ΔLVFS), compared with those in the AMI control group. Compared with the group treated with MSCs alone, APN combined with MSCs (APN + MSCs) treatment

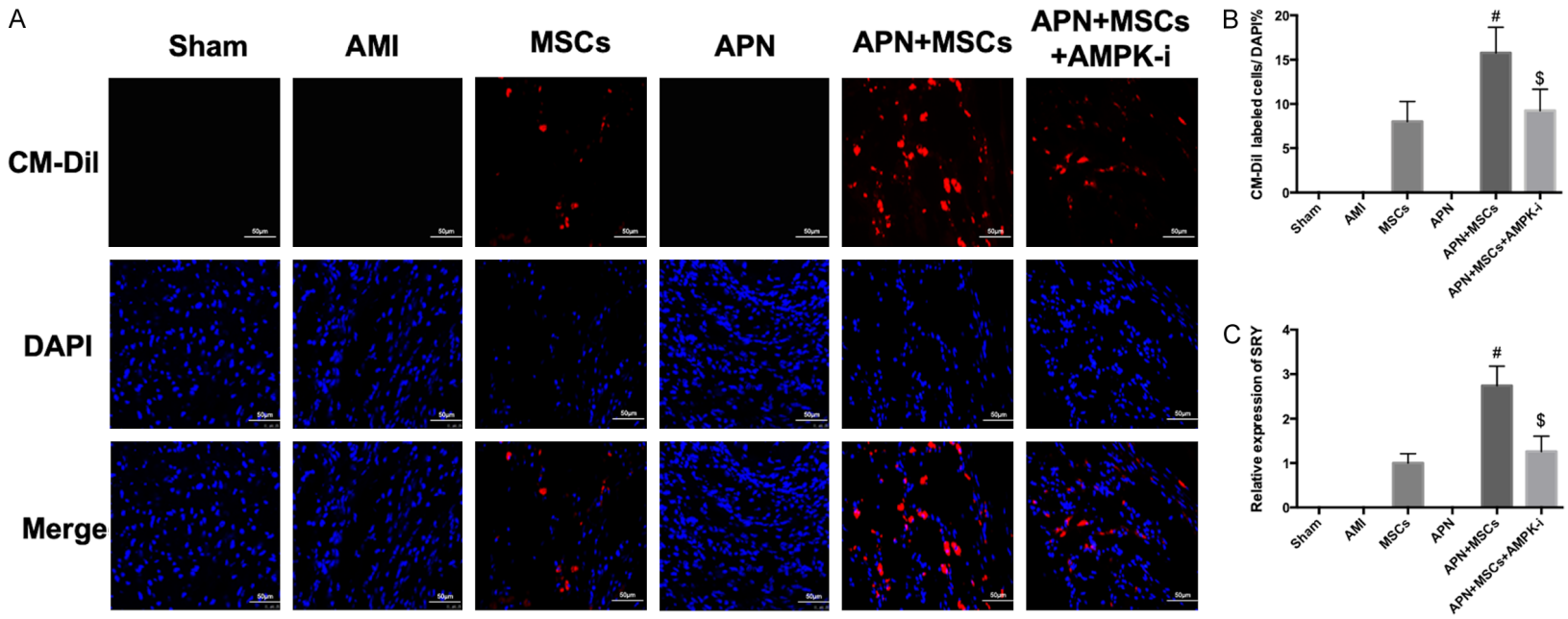

Figure 1. Engraftment and survival of transplanted MSCs labeled with CM-DiI. A. Representative image of CM-DiI-labeled cells in the peri-infarcted myocardium at 4 weeks after AMI (×600). Scale bar =50 μm. B. Quantitation of CM-DiI-labeled cells in each high-power field (HPF) of the peri-infarcted myocardium in each group. C. qPCR analysis of the expression of the sex-determining region of the Y chromosome (SRY) gene to assess the survival of the implanted MSCs. The number of MSCs in the APN + MSCs group was markedly increased compared with that in the MSCs-only group and was significantly decreased following AMPK inhibitor treatment. n=10 in each group. $^{\#}P<0.05$ compared with MSCs group; $^{\$}P<0.05$ compared with APN + MSCs group. AMI: acute myocardial infarction; APN: adiponectin; MSCs: mesenchymal stem cells; AMPK: adenosine monophosphate-activated protein kinase; CM-DiI: 1,1'-dioctadecyl-3,3,3',3'-tetramethylindocarbocyanine perchlorate; DAPI: 4'6-diamidino-2-phenylindole dihydrochloride.

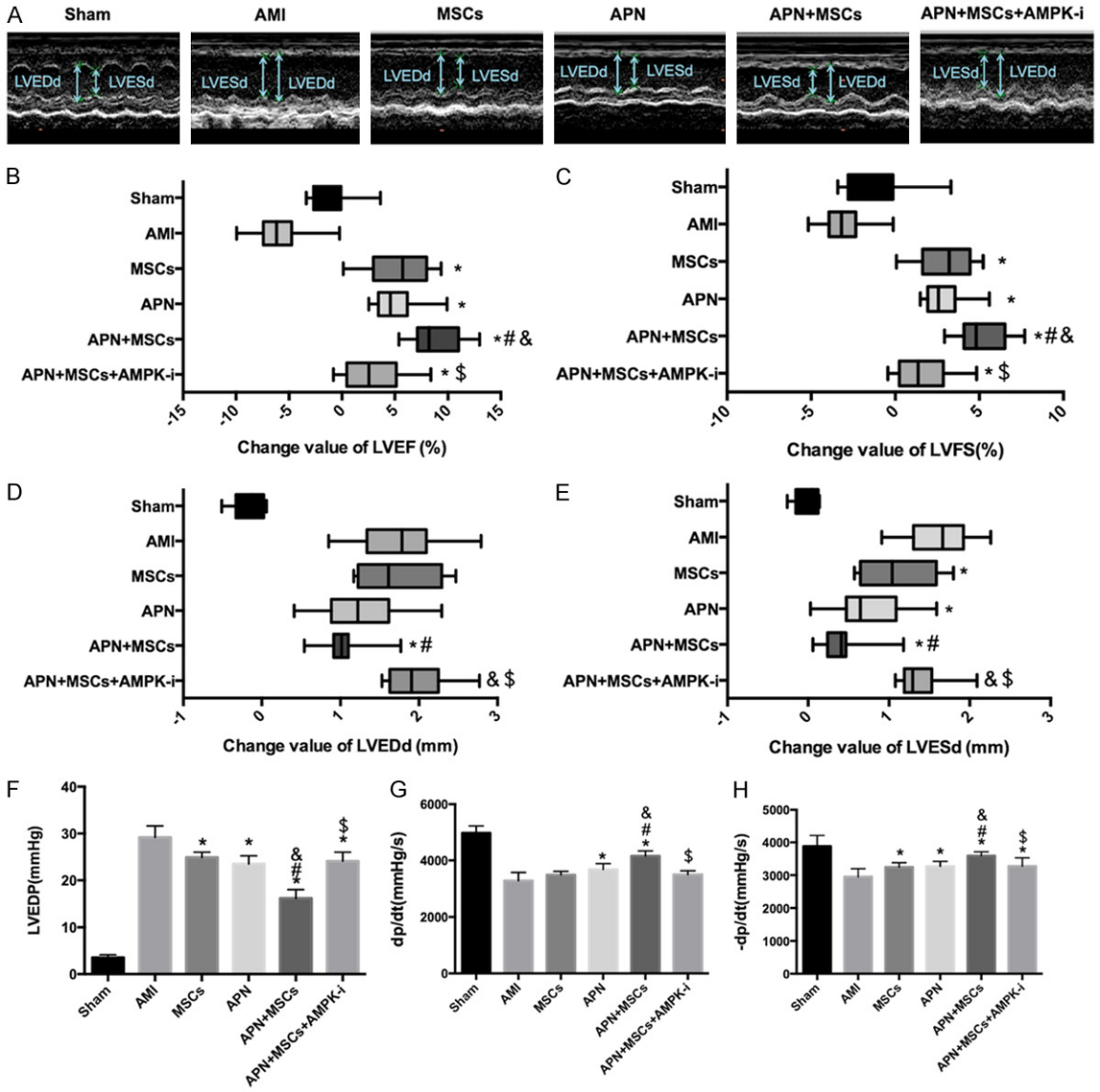

Figure 2. Assessments of cardiac function with echocardiography and left heart catheterization. A. Representative images of M-mode echocardiography at 4 weeks post-AMI. B-E. The changes in the values of LVEF, LVFS, LVEDd, and LVESd from baseline (1 week post-AMI) to the endpoint (4 weeks post-AMI). F-H. The values of LVEDP, dp/dt_{max}, and $-dp/dt_{max}$ detected at the endpoint. At the endpoint, the values for changes in LVEF, LVFS, dp/dt_{max} and $-dp/dt_{max}$ in APN + MSCs group were significantly improved compared with those in the MSCs-only group, while the values for changes in LVEDd, LVESd, and LVEDP were all dramatically reduced, all of which were significantly abrogated following treatment with the AMPK inhibitor. n=10 for each group. $^{*}P<0.05$ compared with AMI group; $^{\#}P<0.05$ compared with MSCs group; $^{\&}P<0.05$ compared with APN group; $^{\$}P<0.05$ compared with APN + MSCs group. AMI: acute myocardial infarction; APN: adiponectin; MSCs: mesenchymal stem cells; AMPK: adenosine monophosphate-activated protein kinase; LVEF: left ventricular ejection fraction; LVFS: left ventricular fractional shortening; LVEDd: left ventricular end-diastolic dimension; LVESd: left ventricular end-systolic dimension; LVEDP: left ventricular end-diastolic dimension; dp/dt_{max}: left ventricular pressure maximal rate of rise; $-dp/dt_{max}$: left ventricular pressure maximal rate of fall.

induced a more significant improvement in the LVEF (8.77±2.32% vs. 5.32±2.99% with MSCs treatment, $P<0.05$) and LVFS (5.10±1.45% vs. 2.97±1.68% with MSCs treatment, $P<0.05$) (**Figure 2A-C**). Moreover, rats in the APN + MSCs group also exhibited significantly reduced changes in the LVEDd (ΔLVEDd) and LVESd (ΔLVESd) (**Figure 2A**, **2D** and **2E**), indicating the attenuation of ventricular structural remodeling. In addition, the left heart catheterization

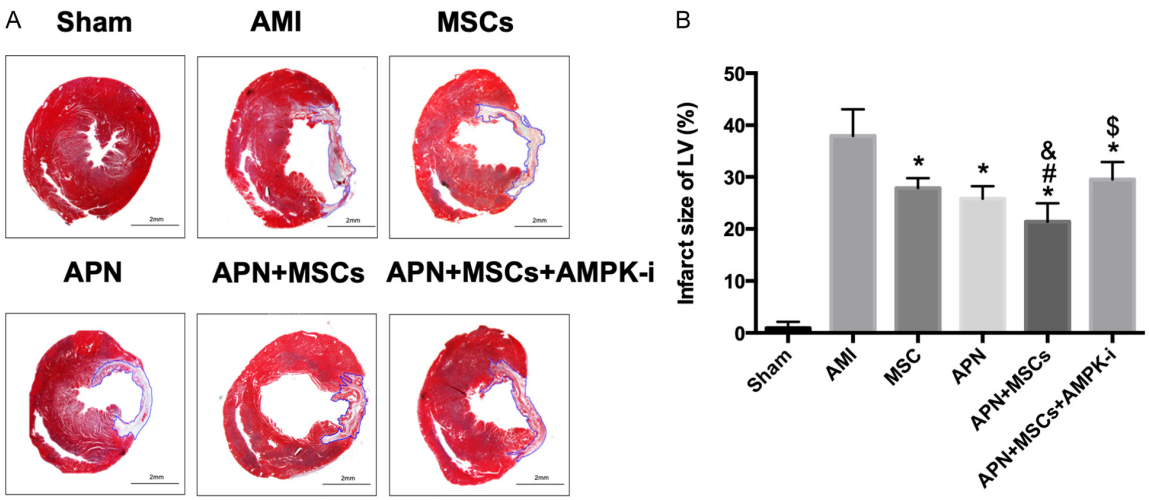

Figure 3. Measurement of the left ventricular infarct size using Masson's trichrome staining. A. Representative images of Masson's trichrome staining in each group. Scale bar =2 mm. B. Quantitative data for the left ventricular infarct size. Compared with all other groups, the APN + MSCs group had the smallest infarct size, which was significantly reversed following AMPK inhibitor treatment. n=10 in each group. $^{*}P<0.05$ compared with AMI group; $^{\#}P<0.05$ compared with MSCs group; $^{\&}P<0.05$ compared with APN group; $^{\$}P<0.05$ compared with APN + MSCs group. AMI: acute myocardial infarction; APN: adiponectin; MSCs: mesenchymal stem cells; AMPK: adenosine monophosphate-activated protein kinase.

results revealed that the combination regimen of APN and MSCs resulted in a significantly reduced LVEDP and an increase in $+dp/dt_{max}$ and $-dp/dt_{max}$ compared with MSCs treatment alone (**Figure 2F-H**; Table S2).

Adjuvant APN treatment with MSCs transplantation reduced the myocardial infarct size

Masson's trichrome staining of the heart tissue was conducted 4 weeks after infarction. As shown in **Figure 3**, transmural infarction existed in all groups of AMI model rats. Thinner anterior walls, dilated LV chambers, severe fibrosis, and large infarct sizes were observed in the hearts of AMI control rats. Compared with the AMI control group, smaller infarct sizes were observed in the hearts of both APN- (25.79±2.42% vs. 37.95±5.12%, $P<0.05$) and MSCs-treated rats (27.87±1.88% vs. 37.95±5.12%, $P<0.05$). The combined delivery of APN and MSCs reduced the infarct size to a greater extent than MSCs transplantation alone (21.38±3.57% vs. 27.87±1.88%, $P<0.05$).

Adjuvant APN treatment with MSCs transplantation inhibited inflammation in the peri-infarct myocardium

A histological analysis was performed at 4 weeks after infarction to assess the infiltration of inflammatory cells (**Figure 4**; Table S3). As shown in **Figure 4A**, H&E staining and immunohistochemistry (IHC) revealed the infiltration of large numbers of inflammatory cells and MHC-II^{+} macrophages in the peri-infarct region of the AMI group, which was inhibited by MSCs or APN treatment alone ($P<0.05$). The combined therapy of APN + MSCs further significantly reduced MHC-II^{+} macrophage infiltration (6.40±2.07% vs. 17.00±1.87%, $P<0.05$) compared with MSCs treatment alone (**Figure 4A**, **4B**). In comparison, IHC staining with an CD206 antibody showed that MSCs significantly increased the number of CD206^{+} macrophages in the peri-infarct region compared with the AMI group ($P<0.05$), while the combined regimen of APN + MSCs further increased the number of CD206^{+} macrophages compared with the MSCs-only group (40.00±4.36% vs. 27.4±4.51%, $P<0.05$) (**Figure 4A**, **4C**). We measured the levels of inflammatory cytokines in the myocardial tissues using ELISAs and qPCR to further quantitatively assess the inflammatory response. As shown in **Figure 4D-I**, compared with the AMI group, the administration of MSCs effectively reduced the levels of the proinflammatory cytokines IL-6 and TNF-α while increasing the level of the anti-inflammatory cytokine IL-10 in the peri-infarct myocardium at both the protein and mRNA lev-

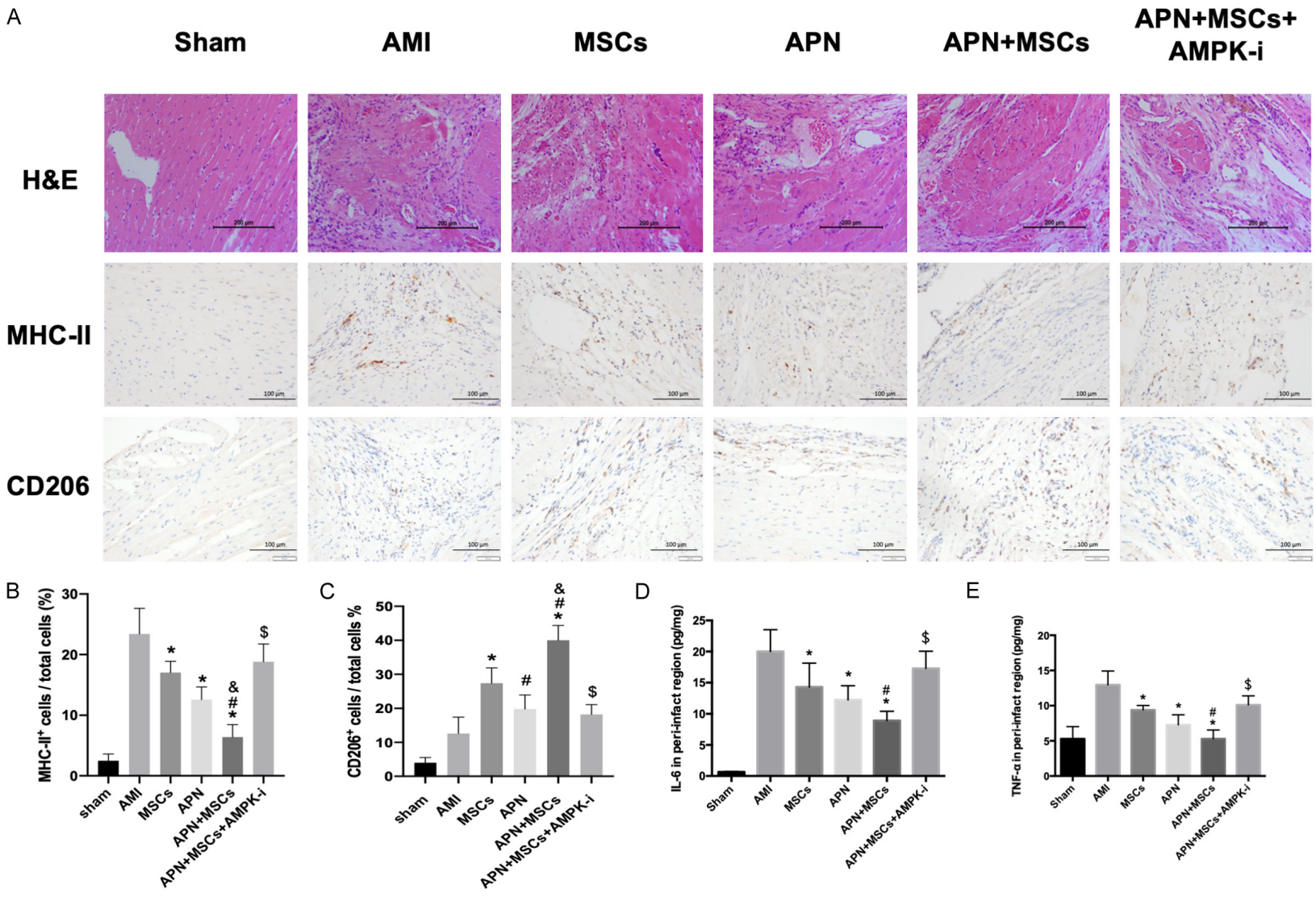
A
Sham
AMI
MSCs
APN
APN+MSCs
APN+MSCs+ AMPK-i
H&E
MHC-II
CD206
B
MHC-II+ cells / total cells (%)
sham
AMI
MSCs
APN
APN+MSCs
APN+MSCs+AMPK-i
C
CD206+ cells / total cells %
D
IL-6 in peri-infact region (pg/mg)
E
TNF-α in peri-infact region (pg/mg)

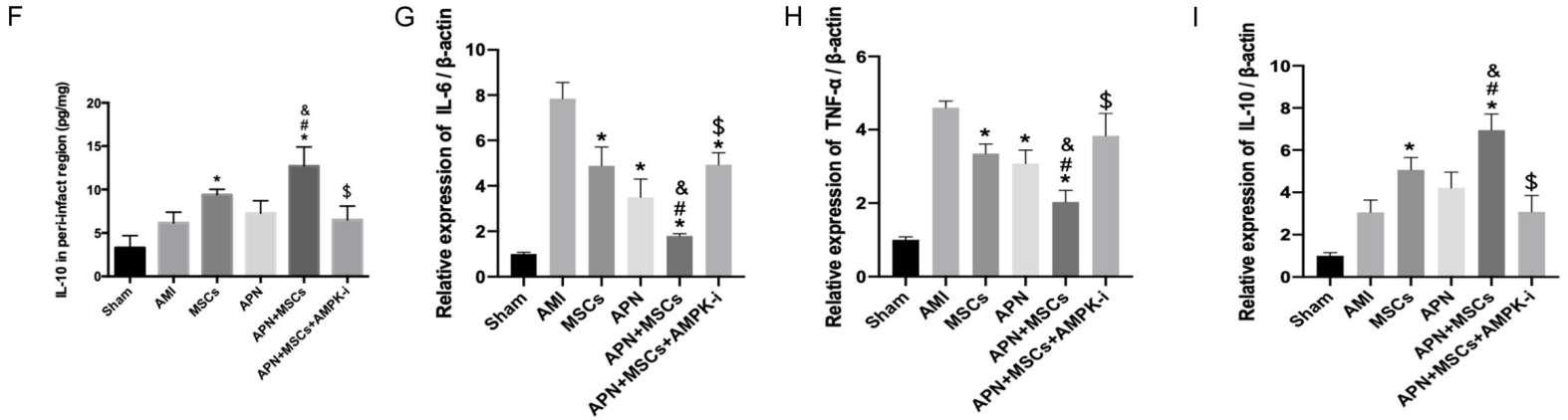

Figure 4. Assessments of the inflammatory response in each group. A. Representative images of H&E staining and MHC-II and CD206 immunohistochemistry in each group (×200). Scale bars =200 μm (H&E) and 100 μm (MHC-II and CD206). B. Quantitative data for the number of MHC-II$^+$ macrophages. C. Quantitative data for the number of CD206$^+$ macrophages. APN + MSCs significantly reduced the infiltration of MHC-II$^+$ macrophages while increasing the number of infiltrating CD206$^+$ macrophages. These effects were significantly reversed following AMPK inhibitor treatment. D-F. Measurement of IL-6, TNF-α, and IL-10 levels in the peri-infarct myocardium using ELISAs. G-I. Levels of the IL-6, TNF-α, and IL-10 mRNAs were measured using quantitative PCR methods. All results were normalized to β-actin. APN + MSCs significantly reduced the levels of the proinflammatory cytokines IL-6 and TNF-α while increasing the level of the anti-inflammatory cytokine IL-10. These effects were significantly reversed by the AMPK inhibitor treatment. n=10 in each group. $^*P$<0.05 compared with AMI group; $^\#P$<0.05 compared with MSCs group; $^\&P$<0.05 compared with APN group; $^\$P$<0.05 compared with APN + MSCs group. AMI: acute myocardial infarction; APN: adiponectin; MSCs: mesenchymal stem cells; AMPK: adenosine monophosphate-activated protein kinase; IL: interleukin; TNF: tumor necrosis factor.

els (P<0.05). Combined administration of APN and MSCs further significantly decreased the protein and mRNA levels of IL-6 (8.90±1.51 pg/mg vs. 4.31±3.82 pg/mg for the protein, P<0.05; 1.80±0.10 vs. 4.88±0.80 for the mRNA, P<0.05) and TNF-α (5.29±1.26 pg/mg vs. 9.39±0.63 pg/mg for the protein, P<0.05; 2.03±0.32 vs. 3.35±0.26 for the mRNA, P< 0.05) and increased the level of IL-10 (12.29±2.20 pg/mg vs. 9.40±0.65 pg/mg for the protein, P<0.05; 6.94±0.76 vs. 5.06±0.58 for the mRNA, P<0.05) compared with MSCs treatment alone.

Adjuvant APN treatment with MSCs transplantation inhibited cardiomyocyte and MSCs apoptosis in the peri-infarct region

TUNEL staining was performed to evaluate the apoptosis of cardiomyocytes and transplanted MSCs. As shown in **Figure 5A** and **5B**, AMI-induced cardiomyocyte apoptosis at the border zone of the infarcted myocardium was significantly reduced after the transplantation of MSCs (P<0.05). The administration of APN alone was also associated with a decreased number of apoptotic cardiomyocytes in the peri-infarct myocardium (P<0.05). Combined therapy with APN and MSCs, which resulted in substantially improved engraftment of MSCs, induced a more significant reduction in the number of apoptotic cardiomyocytes compared with MSCs treatment alone (13.57±4.60% vs. 24.10±2.55%, P<0.05). Notably, consistent with the antiapoptotic effect of APN on MSCs *in vitro*, the TUNEL results also showed a significant reduction in the apoptosis of transplanted MSCs in the APN + MSCs group compared with the group treated with MSCs alone *in vivo* (27.57±3.95% vs. 38.30±4.98%, P< 0.05) (**Figure 5C**).

Adjuvant APN treatment with MSCs transplantation enhanced arteriogenesis and angiogenesis in the peri-infarct myocardium

Immunostaining for the smooth muscle cell marker α-smooth-muscle actin (α-SMA) and the endothelial cell marker CD31 was performed 4 weeks after AMI to assess arteriogenesis and angiogenesis in the peri-infarct myocardium, respectively. As shown in **Figure 6**, the numbers of both α-SMA- and CD31-positive vessels in the MSCs transplantation group were markedly increased compared with those in the AMI group (P<0.05). Moreover, combined administration of APN and MSCs further increased the numbers of α-SMA- (13.80± 3.11 vs. 7.60±1.52, P<0.05) and CD31-positive vessels (23.20±6.06 vs. 12.80±1.48, P<0.05) compared with MSCs transplantation alone.

APN enhanced the therapeutic effect of MSCs transplantation partially through the AMPK pathway

We used an AMPK inhibitor, Compound C and performed Western blot analysis to assess AMPK phosphorylation and investigate the mechanism by which APN + MSCs exerted the aforementioned cardioprotective effects. As shown in **Figure 7**, APN significantly increased AMPK phosphorylation in the peri-infarct cardiomyocytes and myocardial fibroblasts. As shown in both the immunohistochemistry and Western blot analyses, the combined therapy with APN and MSCs further increased AMPK phosphorylation, which was markedly reversed by Compound C. Furthermore, the increased survival of MSCs induced by APN was attenuated following the administration of Compound C (P<0.05), which implied the potential role of AMPK in this process. Moreover, the beneficial effects of APN combined with MSCs on restoring cardiac function, reducing the infarct size, inhibiting inflammation and apoptosis, and enhancing arteriogenesis and angiogenesis were all strikingly diminished following the administration of the AMPK inhibitor (**Figures 1-6**; Table S4), indicating that these abovementioned beneficial effects of APN + MSCs treatment were mainly attributed to AMPK pathway activation.

Discussion

The limited engraftment and low survival rate of transplanted MSCs in the peri-infarct myocardium are the primary barriers that limit the effectiveness of cell therapy [8, 28, 29]. Based on our previous *in vitro* study which showed that APN inhibited the apoptosis of MSCs under induced ischemic conditions [20], the present study further supported that APN significantly increased the survival of transplanted MSCs in the peri-infarct myocardium *in vivo*, and with improved cardiac function, attenuated ventricular remodeling and reduced infarct size. At the cellular level, the underlying mechanisms might involve the inhibition of inflamma-

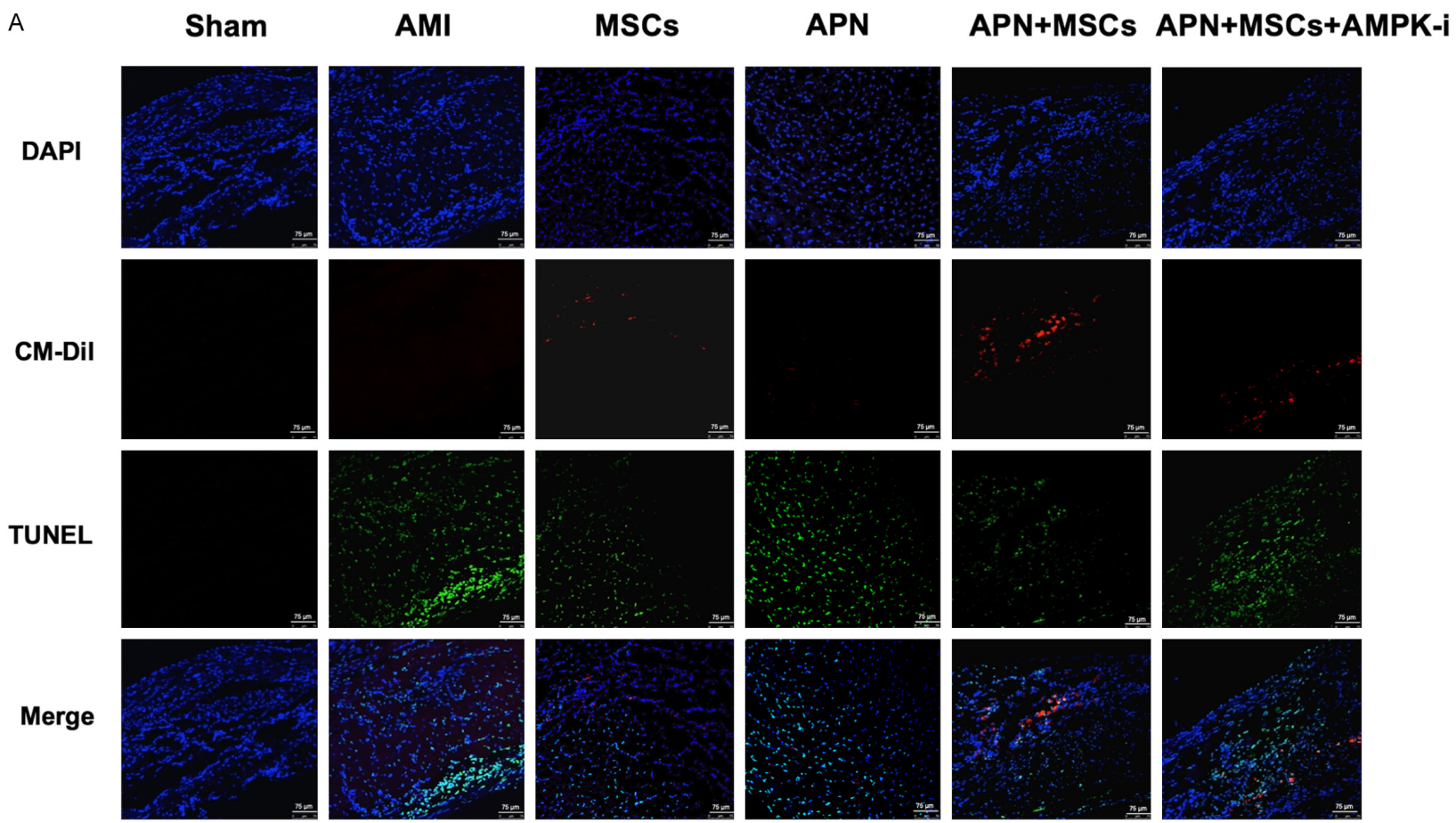
A
Sham
AMI
MSCs
APN
APN+MSCs
APN+MSCs+AMPK-i
DAPI
CM-DiI
TUNEL
Merge

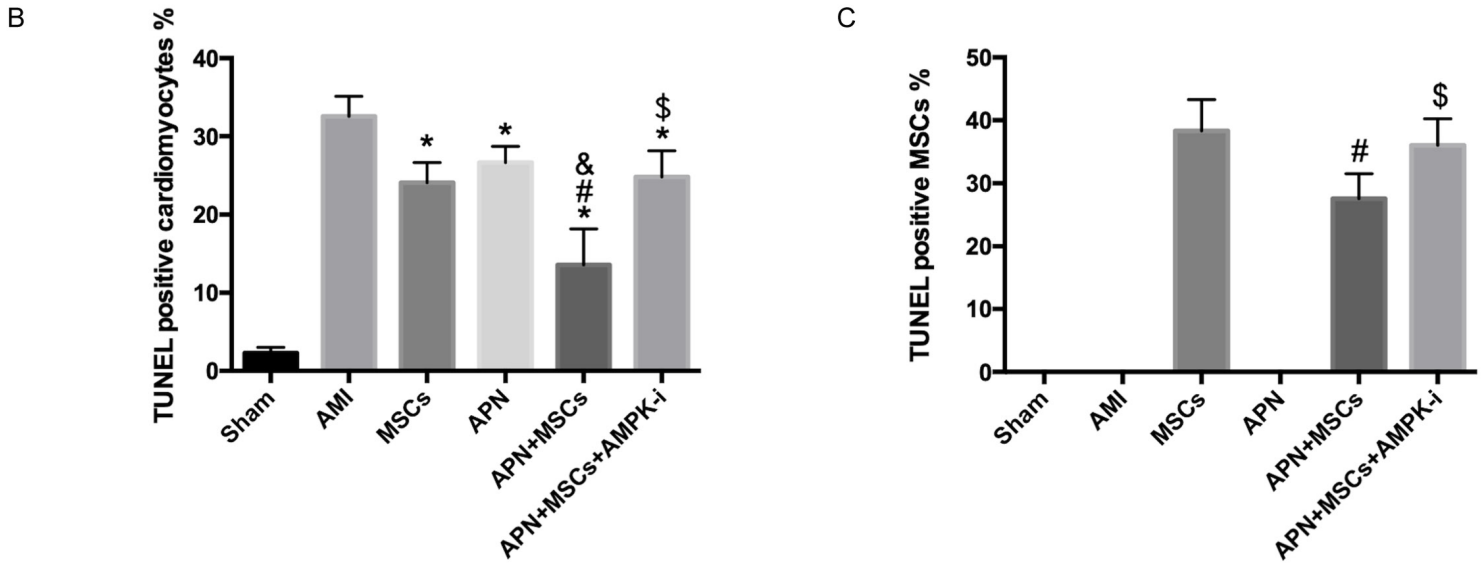

Figure 5. Assessments of cardiomyocyte and MSCs apoptosis using TUNEL staining. A. Representative images of TUNEL staining in each group (×200). Scale bar =75 μm. B. Ratio of apoptotic cardiomyocytes (TUNEL positive alone) to total cells in each group. C. The ratio of apoptotic MSCs (both CM-DiI- and TUNEL-positive) to total cells in each group. The APN + MSCs group exhibited significant reductions in the numbers apoptotic cardiomyocytes and MSCs, both of which were significantly reversed by treatment with an AMPK inhibitor. $^{*}P<0.05$ compared with AMI group; $^{\#}P<0.05$ compared with MSCs group; $^{\&}P<0.05$ compared with APN group; $^{\$}P<0.05$ compared with APN + MSCs group. AMI: acute myocardial infarction; APN: adiponectin; MSCs: mesenchymal stem cells; AMPK: adenosine monophosphate-activated protein kinase; CM-DiI: 1,1'-dioctadecyl-3,3,3',3'-tetramethylindocarbocyanine perchlorate; DAPI: 4'6-diamidino-2-phenylindole dihydrochloride; TUNEL: TdT-mediated dUTP nick-end labeling.

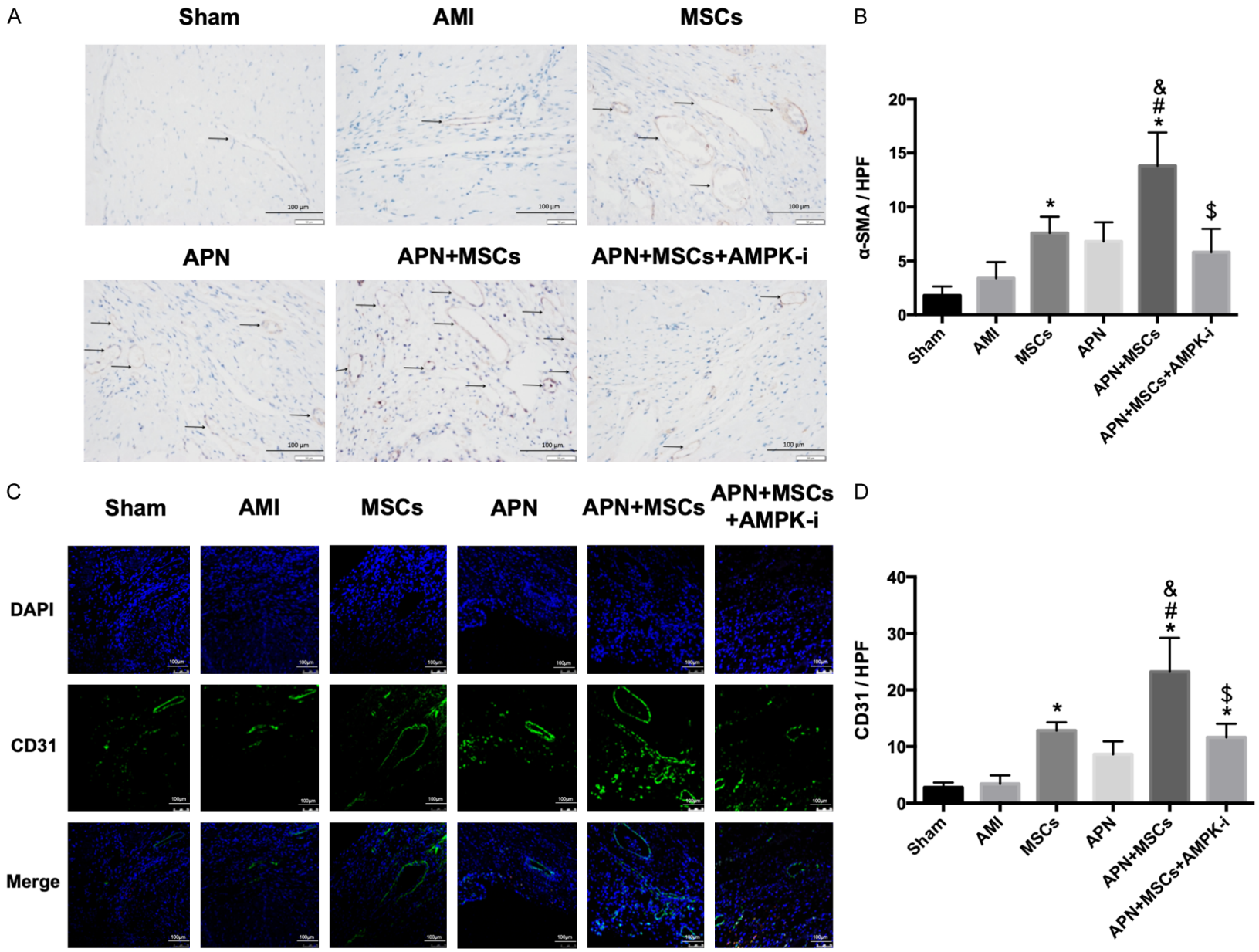
A
Sham
AMI
MSCs
APN
APN+MSCs
APN+MSCs+AMPK-i
B
α-SMA / HPF
20
15
10
5
0
&
#
*
*
$
Sham
AMI
MSCs
APN
APN+MSCs
APN+MSCs+AMPK-i
C
Sham
AMI
MSCs
APN
APN+MSCs
APN+MSCs +AMPK-i
DAPI
CD31
Merge
D
CD31 / HPF
40
30
20
10
0
&
#
*
*
*
$
Sham
AMI
MSCs
APN
APN+MSCs
APN+MSCs+AMPK-i

Figure 6. Arteriogenesis and angiogenesis were evaluated using α-SMA and CD31 staining. A. Representative images of α-SMA staining in the peri-infarct myocardium of each group. Arrow: α-SMA-positive vessels. Scale bar =100 μm. B. Arteriogenesis was evaluated by calculating the number of α-SMA-positive vessels per HPF. C. Representative images of CD31 staining in the peri-infarct myocardium of each group. Scale bar =100 μm. D. Angiogenesis was evaluated by calculating the number of CD31-positive vessels per HPF. APN + MSCs significantly increased arteriogenesis and angiogenesis compared with MSCs alone, changes that were significantly reversed by the AMPK inhibitor treatment. $^{*}P<0.05$ compared with AMI group; $^{\#}P<0.05$ compared with MSCs group; $^{\&}P<0.05$ compared with APN group; $^{\$}P<0.05$ compared with APN + MSCs group. AMI: acute myocardial infarction; APN: adiponectin; MSCs: mesenchymal stem cells; AMPK: adenosine monophosphate-activated protein kinase; DAPI: 4'6-diamidino-2-phenylindole dihydrochloride; α-SMA: α-smooth muscle actin.

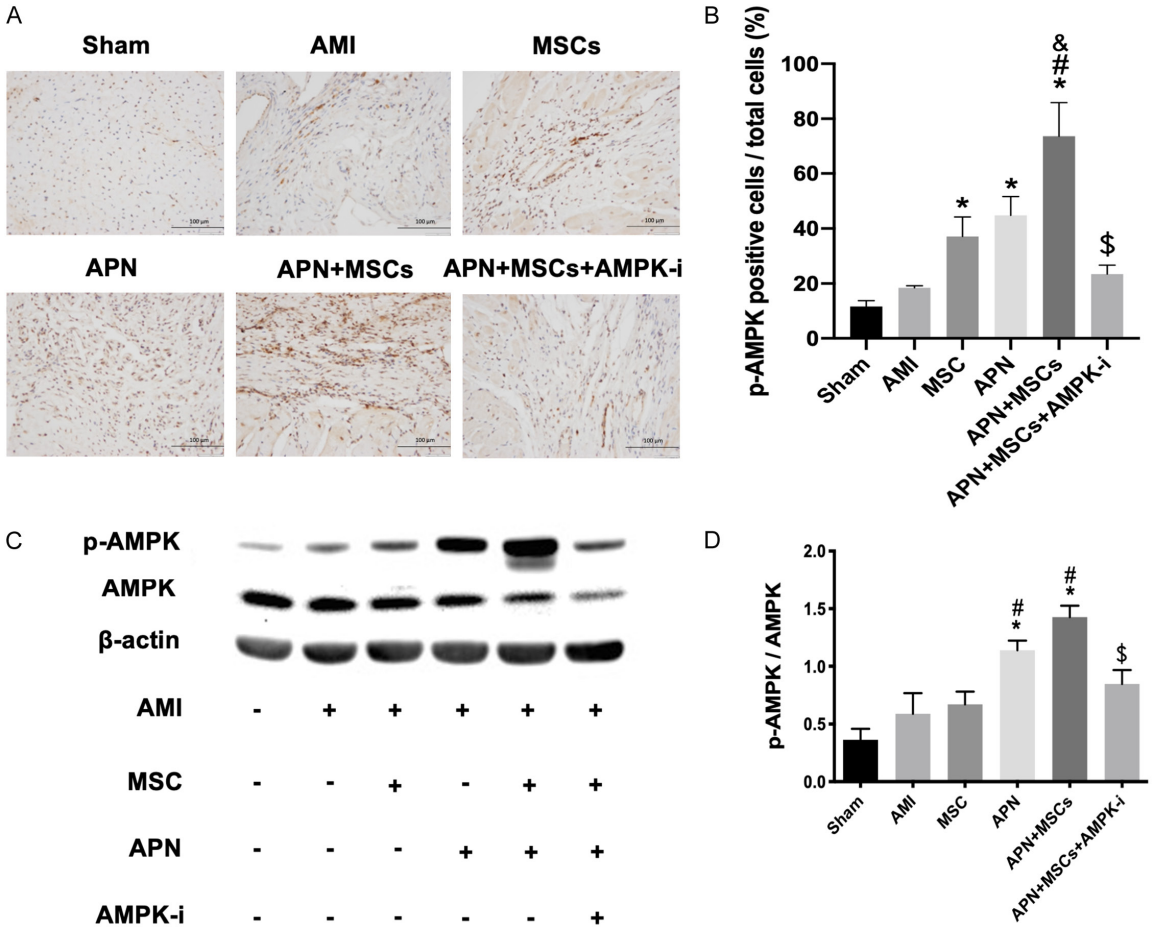

Figure 7. AMPK phosphorylation was assessed with immunohistochemistry and Western blotting. A. Representative images of p-AMPK staining in the peri-infarct myocardium of each group (×200). Scale bar =100 μm. B. Quantitation of the positive signal for AMPK phosphorylation. C. Representative images of p-AMPK and AMPK levels in each group. D. Quantitative data for p-AMPK/AMPK in each group. APN significantly increased AMPK phosphorylation in the myocardium. Combined therapy with APN and MSCs further increased AMPK phosphorylation, which was markedly reversed by an AMPK inhibitor. $^{*}P<0.05$ compared with AMI group; $^{\#}P<0.05$ compared with MSCs group; $^{\&}P<0.05$ compared with APN group; $^{\$}P<0.05$ compared with APN + MSCs group. AMI: acute myocardial infarction; APN: adiponectin; MSCs: mesenchymal stem cells; AMPK: adenosine monophosphate-activated protein kinase.

tion, especially the promotion of the anti-inflammatory phenotype of macrophages, a reduction in cardiomyocyte apoptosis, and increases in arteriogenesis and angiogenesis in the peri-infarct myocardium. Furthermore, at the molecular level, the above mentioned beneficial effects at least partially depended on the activation of the AMPK pathway (**Figure 8**).

In addition to the well-established metabolic regulatory and cardioprotective effects, APN also exerts some beneficial effects on facilitat-

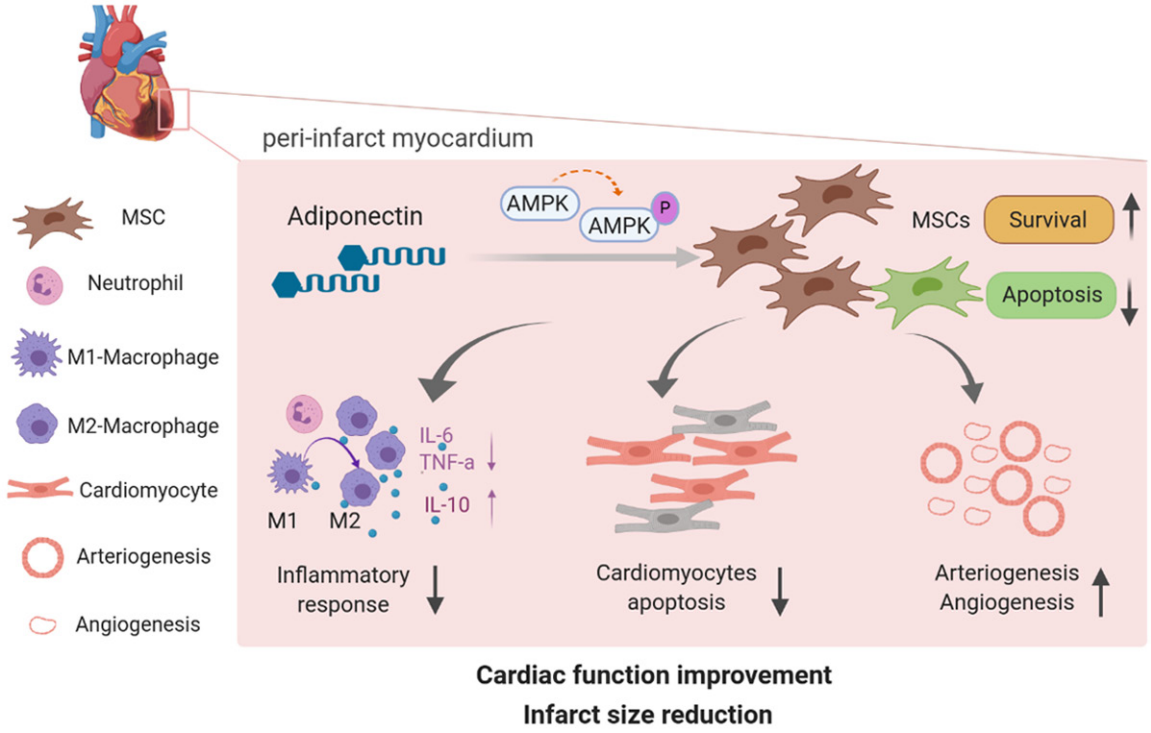

Figure 8. Schematic diagram of the effects of APN on MSCs survival and therapeutic efficacy in AMI. Adiponectin (APN) increased the survival rate of transplanted mesenchymal stem cells (MSCs) by activating the AMPK pathway. This change augmented the cardioprotective effects of MSCs on suppressing the inflammatory response, inhibiting cardiomyocyte apoptosis, and enhancing arteriogenesis and angiogenesis in the peri-infarct myocardium. These beneficial effects subsequently resulted in markedly improved cardiac function and a decreased infarct size after acute myocardial infarction.

ing MSCs osteogenesis under osteogenic induction conditions [30, 31], enhancing MSCs resistance to flow shear stress [32], and regulating the mobilization and recruitment of MSCs to participate in tissue repair and regeneration [19, 33]. In the field of cardiac repair, a recent study showed that APN stimulates MSCs exosome biogenesis and secretion to improve left ventricular cardiac function in a pressure-overload model [22]. Consistent with our previous *in vitro* study, it indicated that APN inhibited the apoptosis of MSCs under induced ischemic conditions [20]. Our present study showed that the engraftment and survival of MSCs in the peri-infarct myocardium were significantly increased following APN treatment, while markedly improved cardiac function and a decreased infarct size at 4 weeks after AMI were observed. This result was consistent with our previous studies showing that interventions aimed at improving the quality of local microenvironments to facilitate survival and the biological behavior of transplanted cells is effective and clinically practicable [24, 26, 34].

In addition, the present study revealed that the remarkable beneficial effects of APN on MSCs survival and the subsequent cardiac repairs were mediated by AMPK activation. This is consistent with our previous *in vitro* study which showed that AMPK mediated the inhibitory effects of APN on MSCs apoptosis [20]. APN induces extracellular calcium influx by binding adiponectin receptor 1 (AdipoR1) and activates calcium/calmodulin-dependent protein kinase kinase (CaMKK), which is necessary for subsequent direct phosphorylation of AMPK-α (Thr172) [35]. AMPK activation by APN is critical for cellular responses to metabolic stress involving energy generation and consumption [23, 35-37], thus mediating the protective effects of APN on MSCs survival [20, 32]. Our data revealed that APN induced sustained phosphorylation of AMPK in the myocardium at 4 weeks post-AMI, and the application of an AMPK inhibitor significantly inhibited the protective effect of APN. Taken together, these findings strongly indicated that the AMPK pathway was required for the protective effects of

APN on MSCs survival and cardiac repair. This study represents the first attempt to elucidate the signals involved in APN-mediated protective properties in MSCs in the infarcted myocardial microenvironment.

The present study also suggested that the cellular mechanisms underlying the striking therapeutic effects were mainly associated with anti-inflammatory and anti-apoptotic activities and the enhancement of arteriogenesis and angiogenesis through the synergistic effects of APN treatment and MSCs transplantation.

Macrophage infiltration participated in the postmyocardial wound healing process. In particular, the polarization of macrophages (a proper shift toward M2 macrophages) would help prevent excessive scar formation and remodeling, which might have significant clinical implications for attenuating inflammatory cytokine production [38, 39]. In recent years, the therapeutic properties of stem cells have clearly been shown to be related to their capacity to modulate inflammatory and immune responses [5, 40-42]. MSCs have been shown to switch macrophages into a regulatory phenotype *in vitro* [43] and promote the phenotype of infiltrated macrophages to shift to anti-inflammatory M2 phenotype and modulate the immunological environment after myocardial infarction *in vivo* [44]. In our study, we investigated changes in the expression of macrophage surface markers (MHC-II and CD206) with immunohistochemistry and secretory markers (IL-6, TNF-α, and IL-10) with ELISAs and qPCR. Consistent with these previous studies, our present study also revealed that MSCs transplantation increased the number of M2 ($CD206^+$) macrophages, while the combined administration of APN and MSCs further enhanced the macrophage shift to the M2 phenotype. These results were confirmed by a decrease in the levels of the inflammatory cytokines IL-6 and TNF-α and an increase in the level of the anti-inflammatory cytokine IL-10. APN functions as a direct regulator of the macrophage phenotype, favoring the switch from a proinflammatory M1-like state to an anti-inflammatory M2-like state [45]. These anti-inflammatory effects of APN on macrophages through an as-yet-unidentified mechanism presumably augment its direct actions on tissues that are mediated by the upregulation of AMPK signaling [45]. Thus, the ability of APN to promote an anti-inflammatory phenotype in macrophages modified the unfavorable cytokine-rich environment to promote the survival of therapeutic MSCs.

In addition, both MSCs and APN protect cardiomyocytes from apoptosis [14, 36], which is the main factor contributing to massive cardiomyocyte death observed in the infarcted heart. Consistent with these findings, both MSCs and APN treatments helped decrease the number of apoptotic cardiomyocytes in the peri-infarct myocardium, whereas adjuvant APN treatment with MSCs further profoundly suppressed apoptosis in the present study. In particular, our results also showed a significant reduction in the apoptosis of transplanted MSCs in the APN combined with MSCs group compared with the MSCs-only group, which was inconsistent with our previous study showing that APN inhibited the apoptosis of MSCs under hypoxic and serum-deprivation conditions *in vitro*. In addition, the maintenance of vessel density preserved cardiac function and protected against ventricular remodeling in the AMI model. Proangiogenesis is a well-known paracrine mechanism through which MSCs exert cardioprotective effects [46]. APN also exerts a proangiogenic effect, which might be attributed to the increased migration and function of endothelial progenitor cells [47, 48]. In the present study, adjuvant APN treatment with MSCs transplantation promoted arteriogenesis and angiogenesis in peri-infarct regions, which might further help to repair the damaged heart.

We acknowledge that this study had some limitations. First, only one time point at 4 weeks post AMI was observed. A time course with more time points showing the cardiac repair process would be preferred in future studies. Additionally, we did not investigate the distributions of MSCs in organs other than the heart. Considering the retention of MSCs in the lungs, the results would be more convincing if we determined the relative numbers of MSCs detected in the myocardium to the number of cells detected in other organs. Finally, a genetically mismatched transplantation experiment in AMI animal models does not represent the situation of clinical practice in the real world. Further studies are required in the future.

Conclusions

In conclusion, this study is the first to document experimental evidence showing that APN treatment effectively increased the survival of transplanted MSCs in the infarcted tissue, accompanied by functional benefits resulting from cell transplantation. The data from the present study suggested that a combination of APN and MSCs transplantation might exert synergistic effects on the repair of myocardial function and morphology postinfarction and might represent a promising strategy for cardiac repair after AMI.

Acknowledgements

This work was supported by grants from the National Natural Science Foundation of China (81700362 and 81300112) and 863 Program of China (2011AA020110).

Disclosure of conflict of interest

None.

Address correspondence to: Dr. Yue-Jin Yang, Fuwai Hospital, No. 167 Beilishi Road, Xicheng District, Beijing 100037, China. Tel: +86-10-88398760; Fax: +86-10-68351786; E-mail: yangyuejinfw@126.com

References

[1] Desgres M and Menasche P. Clinical translation of pluripotent stem cell therapies: challenges and considerations. Cell Stem Cell 2019; 25: 594-606.

[2] Goradel NH, Hour FG, Negahdari B, Malekshahi ZV, Hashemzehi M, Masoudifar A and Mirzaei H. Stem cell therapy: a new therapeutic option for cardiovascular diseases. J Cell Biochem 2018; 119: 95-104.

[3] Lemcke H, Voronina N, Steinhoff G and David R. Recent progress in stem cell modification for cardiac regeneration. Stem Cells Int 2018; 2018: 1909346.

[4] Shafei AE, Ali MA, Ghanem HG, Shehata AI, Abdelgawad AA, Handal HR, Talaat KA, Ashaal AE and El-Shal AS. Mesenchymal stem cell therapy: a promising cell-based therapy for treatment of myocardial infarction. J Gene Med 2017; 19: e2995.

[5] Luger D, Lipinski MJ, Westman PC, Glover DK, Dimastromatteo J, Frias JC, Albelda MT, Sikora S, Kharazi A, Vertelov G, Waksman R and Epstein SE. Intravenously delivered mesenchymal stem cells: systemic anti-inflammatory effects improve left ventricular dysfunction in acute myocardial infarction and ischemic cardiomyopathy. Circ Res 2017; 120: 1598-1613.

[6] Afzal MR, Samanta A, Shah ZI, Jeevanantham V, Abdel-Latif A, Zuba-Surma EK and Dawn B. Adult bone marrow cell therapy for ischemic heart disease: evidence and insights from randomized controlled trials. Circ Res 2015; 117: 558-575.

[7] Liu B, Duan CY, Luo CF, Ou CW, Sun K, Wu ZY, Huang H, Cheng CF, Li YP and Chen MS. Effectiveness and safety of selected bone marrow stem cells on left ventricular function in patients with acute myocardial infarction: a meta-analysis of randomized controlled trials. Int J Cardiol 2014; 177: 764-770.

[8] Khodayari S, Khodayari H, Amiri AZ, Eslami M, Farhud D, Hescheler J and Nayernia K. Inflammatory microenvironment of acute myocardial infarction prevents regeneration of heart with stem cells therapy. Cell Physiol Biochem 2019; 53: 887-909.

[9] Taylor DA, Chandler AM, Gobin AS and Sampaio LC. Maximizing cardiac repair: should we focus on the cells or on the matrix? Circ Res 2017; 120: 30-32.

[10] Achari AE and Jain SK. Adiponectin, a therapeutic target for obesity, diabetes, and endothelial dysfunction. Int J Mol Sci 2017; 18: 1321.

[11] Fang H and Judd RL. Adiponectin regulation and function. Compr Physiol 2018; 8: 1031-1063.

[12] Li J, Lu W, Ye J, Han Y, Chen H and Wang L. Association between expression of AMPK pathway and adiponectin, leptin, and vascular endothelial function in rats with coronary heart disease. Eur Rev Med Pharmacol Sci 2020; 24: 905-914.

[13] Zhu Q, Li H, Xie X, Chen X, Kosuru R, Li S, Lian Q, Cheung CW, Irwin MG, Ge RS and Xia Z. Adiponectin facilitates postconditioning cardioprotection through both AMPK-dependent nuclear and AMPK-independent mitochondrial STAT3 activation. Oxid Med Cell Longev 2020; 2020: 4253457.

[14] Shibata R, Sato K, Pimentel DR, Takemura Y, Kihara S, Ohashi K, Funahashi T, Ouchi N and Walsh K. Adiponectin protects against myocardial ischemia-reperfusion injury through AMPK- and COX-2-dependent mechanisms. Nat Med 2005; 11: 1096-1103.

[15] Shibata R, Izumiya Y, Sato K, Papanicolaou K, Kihara S, Colucci WS, Sam F, Ouchi N and Walsh K. Adiponectin protects against the development of systolic dysfunction following myocardial infarction. J Mol Cell Cardiol 2007; 42: 1065-1074.

[16] Fiaschi T, Magherini F, Gamberi T, Modesti PA and Modesti A. Adiponectin as a tissue regenerating hormone: more than a metabolic function. Cell Mol Life Sci 2014; 71: 1917-1925.
[17] Masamoto Y, Arai S, Sato T, Kubota N, Takamoto I, Kadowaki T and Kurokawa M. Adiponectin enhances quiescence exit of murine hematopoietic stem cells and hematopoietic recovery through mTORC1 potentiation. Stem Cells 2017; 35: 1835-1848.
[18] Ren Y, Li Y, Yan J, Ma M, Zhou D, Xue Z, Zhang Z, Liu H, Yang H, Jia L, Zhang L, Zhang Q, Mu S, Zhang R and Da Y. Adiponectin modulates oxidative stress-induced mitophagy and protects C2C12 myoblasts against apoptosis. Sci Rep 2017; 7: 3209.
[19] Yu L, Tu Q, Han Q, Zhang L, Sui L, Zheng L, Meng S, Tang Y, Xuan D, Zhang J, Murray D, Shen Q, Cheng J, Kim SH, Dong LQ, Valverde P, Cao X and Chen J. Adiponectin regulates bone marrow mesenchymal stem cell niche through a unique signal transduction pathway: an approach for treating bone disease in diabetes. Stem Cells 2015; 33: 240-252.
[20] Tian XQ, Yang YJ, Li Q, Huang PS, Li XD, Jin C, Qi K, Jiang LP and Chen GH. Globular adiponectin inhibits the apoptosis of mesenchymal stem cells induced by hypoxia and serum deprivation via the adipor1-mediated pathway. Cell Physiol Biochem 2016; 38: 909-925.
[21] de Meester C, Timmermans AD, Balteau M, Ginion A, Roelants V, Noppe G, Porporato PE, Sonveaux P, Viollet B, Sakamoto K, Feron O, Horman S, Vanoverschelde JL, Beauloye C and Bertrand L. Role of AMP-activated protein kinase in regulating hypoxic survival and proliferation of mesenchymal stem cells. Cardiovasc Res 2014; 101: 20-29.
[22] Nakamura Y, Kita S, Tanaka Y, Fukuda S, Obata Y, Okita T, Nishida H, Takahashi Y, Kawachi Y, Tsugawa-Shimizu Y, Fujishima Y, Nishizawa H, Takakura Y, Miyagawa S, Sawa Y, Maeda N and Shimomura I. Adiponectin stimulates exosome release to enhance mesenchymal stem-cell-driven therapy of heart failure in mice. Mol Ther 2020; 28: 2203-2219.
[23] Yan W, Zhang H, Liu P, Wang H, Liu J, Gao C, Liu Y, Lian K, Yang L, Sun L, Guo Y, Zhang L, Dong L, Lau WB, Gao E, Gao F, Xiong L, Wang H, Qu Y and Tao L. Impaired mitochondrial biogenesis due to dysfunctional adiponectin-AMPK-PGC-1alpha signaling contributing to increased vulnerability in diabetic heart. Basic Res Cardiol 2013; 108: 329.
[24] Xu J, Xiong YY, Li Q, Hu MJ, Huang PS, Xu JY, Tian XQ, Jin C, Liu JD, Qian L and Yang YJ. Optimization of timing and times for administration of atorvastatin-pretreated mesenchymal stem cells in a preclinical model of acute myocardial infarction. Stem Cells Transl Med 2019; 8: 1068-1083.
[25] Zheng JH, Zhang JK, Kong DS, Song YB, Zhao SD, Qi WB, Li YN, Zhang ML and Huang XH. Quantification of the CM-DiI-labeled human umbilical cord mesenchymal stem cells migrated to the dual injured uterus in SD rat. Stem Cell Res Ther 2020; 11: 280.
[26] Tian XQ, Yang YJ, Li Q, Xu J, Huang PS, Xiong YY, Li XD, Jin C, Qi K, Jiang LP, Chen GH, Qian L, Liu J and Geng YJ. Combined therapy with atorvastatin and atorvastatin-pretreated mesenchymal stem cells enhances cardiac performance after acute myocardial infarction by activating SDF-1/CXCR4 axis. Am J Transl Res 2019; 11: 4214-4231.
[27] Zhang Q, Wang H, Yang YJ, Dong QT, Wang TJ, Qian HY, Li N, Wang XM and Jin C. Atorvastatin treatment improves the effects of mesenchymal stem cell transplantation on acute myocardial infarction: the role of the RhoA/ROCK/ERK pathway. Int J Cardiol 2014; 176: 670-679.
[28] Hu X, Xu Y, Zhong Z, Wu Y, Zhao J, Wang Y, Cheng H, Kong M, Zhang F, Chen Q, Sun J, Li Q, Jin J, Li Q, Chen L, Wang C, Zhan H, Fan Y, Yang Q, Yu L, Wu R, Liang J, Zhu J, Wang Y, Jin Y, Lin Y, Yang F, Jia L, Zhu W, Chen J, Yu H, Zhang J and Wang J. A large-scale investigation of hypoxia-preconditioned allogeneic mesenchymal stem cells for myocardial repair in nonhuman primates: paracrine activity without remuscularization. Circ Res 2016; 118: 970-983.
[29] Sanganalmath SK and Bolli R. Cell therapy for heart failure: a comprehensive overview of experimental and clinical studies, current challenges, and future directions. Circ Res 2013; 113: 810-834.
[30] Pu Y, Wu H, Lu S, Hu H, Li D, Wu Y and Tang Z. Adiponectin promotes human jaw bone marrow stem cell osteogenesis. J Dent Res 2016; 95: 769-775.
[31] Wang Y, Zhang X, Shao J, Liu H, Liu X and Luo E. Adiponectin regulates BMSC osteogenic differentiation and osteogenesis through the Wnt/beta-catenin pathway. Sci Rep 2017; 7: 3652.
[32] Zhao L, Fan C, Zhang Y, Yang Y, Wang D, Deng C, Hu W, Ma Z, Jiang S, Di S, Qin Z, Lv J, Sun Y and Yi W. Adiponectin enhances bone marrow mesenchymal stem cell resistance to flow shear stress through AMP-activated protein kinase signaling. Sci Rep 2016; 6: 28752.
[33] Pu Y, Wang M, Hong Y, Wu Y and Tang Z. Adiponectin promotes human jaw bone marrow mesenchymal stem cell chemotaxis via CXCL1 and CXCL8. J Cell Mol Med 2017; 21: 1411-1419.
[34] Li N, Yang YJ, Qian HY, Li Q, Zhang Q, Li XD, Dong QT, Xu H, Song L and Zhang H. Intravenous

administration of atorvastatin-pretreated mesenchymal stem cells improves cardiac performance after acute myocardial infarction: role of CXCR4. Am J Transl Res 2015; 7: 1058-1070.

[35] Iwabu M, Yamauchi T, Okada-Iwabu M, Sato K, Nakagawa T, Funata M, Yamaguchi M, Namiki S, Nakayama R, Tabata M, Ogata H, Kubota N, Takamoto I, Hayashi YK, Yamauchi N, Waki H, Fukayama M, Nishino I, Tokuyama K, Ueki K, Oike Y, Ishii S, Hirose K, Shimizu T, Touhara K and Kadowaki T. Adiponectin and AdipoR1 regulate PGC-1alpha and mitochondria by Ca(2+) and AMPK/SIRT1. Nature 2010; 464: 1313-1319.

[36] Konishi M, Haraguchi G, Ohigashi H, Ishihara T, Saito K, Nakano Y and Isobe M. Adiponectin protects against doxorubicin-induced cardiomyopathy by anti-apoptotic effects through AMPK up-regulation. Cardiovasc Res 2011; 89: 309-319.

[37] Huang B, Cheng X, Wang D, Peng M, Xue Z, Da Y, Zhang N, Yao Z, Li M, Xu A and Zhang R. Adiponectin promotes pancreatic cancer progression by inhibiting apoptosis via the activation of AMPK/Sirt1/PGC-1alpha signaling. Oncotarget 2014; 5: 4732-4745.

[38] Gordon S. Alternative activation of macrophages. Nat Rev Immunol 2003; 3: 23-35.

[39] Gordon S and Taylor PR. Monocyte and macrophage heterogeneity. Nat Rev Immunol 2005; 5: 953-964.

[40] Vagnozzi RJ, Maillet M, Sargent MA, Khalil H, Johansen AK, Schwanekamp JA, York AJ, Huang V, Nahrendorf M, Sadayappan S and Molkentin JD. An acute immune response underlies the benefit of cardiac stem-cell therapy. Nature 2019; 577: 105-409.

[41] Huynh K. Stem cell therapy improves heart function by triggering an acute immune response. Nat Rev Cardiol 2019; 17: 69.

[42] Epstein SE, Luger D and Lipinski MJ. Paracrine-mediated systemic anti-inflammatory activity of intravenously administered mesenchymal stem cells: a transformative strategy for cardiac stem cell therapeutics. Circ Res 2017; 121: 1044-1046.

[43] Maggini J, Mirkin G, Bognanni I, Holmberg J, Piazzon IM, Nepomnaschy I, Costa H, Canones C, Raiden S, Vermeulen M and Geffner JR. Mouse bone marrow-derived mesenchymal stromal cells turn activated macrophages into a regulatory-like profile. PLoS One 2010; 5: e9252.

[44] Cho DI, Kim MR, Jeong HY, Jeong HC, Jeong MH, Yoon SH, Kim YS and Ahn Y. Mesenchymal stem cells reciprocally regulate the M1/M2 balance in mouse bone marrow-derived macrophages. Exp Mol Med 2014; 46: e70.

[45] Ohashi K, Parker JL, Ouchi N, Higuchi A, Vita JA, Gokce N, Pedersen AA, Kalthoff C, Tullin S, Sams A, Summer R and Walsh K. Adiponectin promotes macrophage polarization toward an anti-inflammatory phenotype. J Biol Chem 2010; 285: 6153-6160.

[46] Gnecchi M, Zhang Z, Ni A and Dzau VJ. Paracrine mechanisms in adult stem cell signaling and therapy. Circ Res 2008; 103: 1204-1219.

[47] Huang PH, Chen JS, Tsai HY, Chen YH, Lin FY, Leu HB, Wu TC, Lin SJ and Chen JW. Globular adiponectin improves high glucose-suppressed endothelial progenitor cell function through endothelial nitric oxide synthase dependent mechanisms. J Mol Cell Cardiol 2011; 51: 109-119.

[48] Adams V, Heiker JT, Hollriegel R, Beck EB, Woitek FJ, Erbs S, Bluher M, Stumvoll M, Beck-Sickinger AG, Schuler G and Linke A. Adiponectin promotes the migration of circulating angiogenic cells through p38-mediated induction of the CXCR4 receptor. Int J Cardiol 2013; 167: 2039-2046.

Table S1. Cardiac structure and function assessed by echocardiography at baseline and endpoint

Group	Sham	AMI	MSCs	APN	APN + MSCs	APN + MSCs + AMPK-i
LVEDd (mm)						
Baseline	6.69±0.29	6.72±0.39	6.50±0.31	6.76±0.29	6.58±0.30	6.65±0.27
Endpoint	6.52±0.36	8.46±0.47	8.22±0.27	8.01±0.54	7.62±0.23	8.64±0.27
Changes	-0.16±0.19	1.74±0.57	1.72±0.50	1.26±0.57	1.04±0.32$^{*,\#}$	1.98±0.43$^{\&,\$}$
LVESd (mm)						
Baseline	3.65±0.21	5.27±0.23	5.12±0.27	5.29±0.23	5.16±0.21	5.21±0.24
Endpoint	3.64±0.12	6.89±0.33	6.23±0.27	6.05±0.43	5.59±0.21	6.61±0.19
Changes	-0.01±0.15	1.62±0.42	1.11±0.47*	0.76±0.46*	0.43±0.30$^{*,\#}$	1.40±0.32$^{\&,\$}$
LVEF (%)						
Baseline	83.37±3.73	51.48±3.20	51.12±2.11	51.93±2.17	51.66±1.76	51.96±2.49
Endpoint	82.24±3.34	45.69±3.19	56.44±1.79	56.98±2.44	60.43±3.06	54.97±3.22
Changes	-1.13±2.09	-5.79±2.69	5.32±2.99*	5.05±2.18*	8.77±2.32$^{*,\#,\&}$	3.01±2.94$^{*,\$}$
LVFS (%)						
Baseline	45.27±4.01	21.46±1.72	21.24±1.16	21.68±1.18	21.53±0.95	21.70±1.36
Endpoint	43.99±3.55	18.44±1.60	24.21±1.04	24.54±1.42	26.63±1.87	23.39±1.84
Changes	-1.28±2.06	-3.02±1.40	2.97±1.68*	2.86±1.25*	5.10±1.45$^{*,\#,\&}$	1.69±1.68$^{*,\$}$

Baseline refers to 1-week after AMI; endpoint refers to 4-week after AMI. Change values refer to the value at endpoint minus that at baseline. AMI: acute myocardial infarction; APN: adiponectin; MSCs: mesenchymal stem cells; AMPK: adenosine monophosphate-activated protein kinase; LVEF: left ventricular ejection fraction; LVFS: left ventricular fractional shortening; LVEDd: left ventricular end-diastolic dimension; LVESd: left ventricular end-systolic dimension. n=10 for each group. All values are expressed as mean ± SD. $^{*}p<0.05$ compared with AMI group; $^{\#}p<0.05$ compared with MSCs group; $^{\&}p<0.05$ compared with APN group; $^{\$}p<0.05$ compared with APN + MSCs group.

Table S2. Cardiac function evaluated by left heart catheterization at endpoint

	LVEDP (mmHg)	dp/dt (mmHg/s)	-dp/dt (mmHg/s)
Sham	3.55±0.60	4975±250.9	3855±331.0
AMI	29.15±2.47	3285±289.2	2952±244.5
MSCs	24.89±1.13*	3487±125.0	3249±133.5*
APN	23.48±1.75*	3679±209.0*	3273±149.2*
APN + MSCs	16.15±1.86$^{*,\#,\&}$	4157±178.4$^{*,\#,\&}$	3592±120.7$^{*,\#,\&}$
APN + MSCs + AMPK-i	24.10±1.92$^{*,\$}$	3495±135.0$^{\$}$	3277±255.2$^{*,\$}$

AMI: acute myocardial infarction; APN: adiponectin; MSCs: mesenchymal stem cells; AMPK: adenosine monophosphate-activated protein kinase; LVEDP: left ventricular end-diastolic dimension, dp/dtmax: left ventricular pressure maximal rate of rise, -dp/dtmax: left ventricular pressure maximal rate of fall. n=10 for each group. All values are expressed as mean ± SD. $^{*}p<0.05$ compared with AMI group; $^{\#}p<0.05$ compared with MSCs group; $^{\&}p<0.05$ compared with APN group; $^{\$}p<0.05$ compared with APN + MSCs group.

Table S3. Quantitation of MHC-II$^+$ and CD 206$^+$ macrophages infiltration and measurement of IL-6, TNF-α, IL-10 protein and mRNA expressions in the peri-infarct myocardium

	MHC-II$^+$/total cells (%)	CD206$^+$/total cells (%)	IL-6 (pg/mg)	TNF-α (pg/mg)	IL-10 (pg/mg)	IL-6 mRNA	TNF-α mRNA	IL-10 mRNA
Sham	2.48±1.11	4.00±1.58	0.65±0.08	5.29±1.73	3.29±1.40	1.00±0.08	1.00±0.08	1.01±0.15
AMI	23.40±4.22	12.60±4.83	20.01±3.51	12.96±1.96	6.15±1.24	7.85±0.71	4.60±1.81	3.06±0.58
MSCs	17.00±1.87*	27.40±4.51*	14.31±3.82*	9.39±0.63*	9.40±0.65*	4.88±0.82*	3.35±0.26*	5.06±0.58*
APN	12.60±2.07*	19.80±4.15$^\#$	12.24±2.28*	7.27±1.44*	7.25±1.40	3.50±0.80*	3.08±0.36*	4.22±0.74
APN + MSCs	6.40±2.07$^{*,\#,\&}$	40.00±4.36$^{*,\#,\&}$	8.90±1.51$^{*,\#}$	5.29±1.26$^{*,\#}$	12.69±2.20$^{*,\#,\&}$	1.80±0.10$^{*,\#,\&}$	2.03±0.32$^{*,\#,\&}$	6.94±0.76$^{*,\#,\&}$
APN + MSCs + AMPK-i	18.80±2.95$^\$$	18.20±2.86$^\$$	17.29±2.77$^\$$	10.10±1.29$^\$$	6.50±1.58$^\$$	4.92±0.53$^{*,\$}$	3.84±0.61$^\$$	3.08±0.77$^\$$

IL: interleukin; TNF: tumor necrosis factor. n = 10 in each group. $^*p$<0.05 compared with AMI group; $^\#p$<0.05 compared with MSCs group; $^\&p$<0.05 compared with APN group; $^\$p$<0.05 compared with APN + MSCs group.

Table S4. Quantitation of CM-DiI-labeled cells, infarct size, apoptosis of cardiomyocytes and MSCs, angiogenesis and arteriogenesis in the peri-infarct myocardium

	CM-DiI$^+$/DAPI (%)	Infarct size/LV (%)	TUNEL$^+$/DAPI (%)	CM-DiI$^+$TUNEL$^+$/ CM-DiI$^+$ (%)	α-SMA$^+$/HPF	CD31$^+$/HPF
Sham	-	0.89±1.23	2.27±0.76	-	1.80±0.84	2.80±0.84
AMI	-	37.95±5.12	32.55±2.57	-	3.40±1.52	3.40±1.52
MSCs	8.02±2.26	27.87±1.88*	24.10±2.55*	38.3±4.98	7.60±1.52*	12.80±1.48*
APN	-	25.79±2.42*	26.66±2.07*	-	6.80±1.79	8.60±2.30
APN + MSCs	15.78±2.88$^\#$	21.38±3.57$^{*,\#,\&}$	13.57±4.60$^{*,\#,\&}$	27.57±3.95$^\#$	13.80±3.11$^{*,\#,\&}$	23.20±6.06$^{*,\#,\&}$
APN + MSCs + AMPK-i	9.25±2.41$^\$$	29.50±3.38$^{*,\$}$	24.80±3.36$^{*,\$}$	36.00±4.21$^\$$	5.80±2.17$^\$$	11.60±2.41$^{*,\$}$

CM-DiI: 1,1'-dioctadecyl-3,3,3',3'-tetramethylindocarbocyanine perchlorate; DAPI: 4'6-diamidino-2-phenylindole dihydrochloride; TUNEL: terminal-deoxynucleotidyl transferase-mediated dUTP nick end labeling; HPF: high power field; α-SMA: α-smooth muscle actin. $^*p$<0.05 compared with AMI group; $^\#p$<0.05 compared with MSCs group; $^\&p$<0.05 compared with APN group; $^\$p$<0.05 compared with APN + MSCs group.